Catalysis Today 156 (2010) 153–164

Contents lists available at ScienceDirect

Catalysis Today

journal homepage: www.elsevier.com/locate/cattod

On the potential of nickel catalysts for steam reforming in membrane reactors

J.A.Z. Pieterse*, J. Boon, Y.C. van Delft, J.W. Dijkstra, R.W. van den Brink

Energy research Center of the Netherlands, P.O. Box 1, 1755 ZG Petten, The Netherlands

ARTICLE INFO

Article history:
Available online 17 March 2010

Keywords:
Membrane reactor
Catalyst
Nickel
Stability

ABSTRACT

Hydrogen membrane reactors have been identified as a promising option for hydrogen production for power generation from natural gas with pre-combustion decarbonisation. While Pd or Pd-alloy membranes already provide good hydrogen permeances the most suitable catalyst design for steam reforming in membrane reactors (SRMR) is yet to be identified. This contribution aims to provide insight in the suitability of nickel based catalysts in SRMR. The use of nickel (Ni) catalysts would benefit the cost-effectiveness of membrane reactors and therefore its feasibility. For this, the activity of nickel catalysts in SRMR was assessed with kinetics reported in literature. A 1D model was composed in order to compare the hydrogen production rates derived from the kinetics with the rate of hydrogen withdrawal by permeation. Catalyst stability was studied by exposing the catalysts to reformate gas with two different H/C ratios to mimic the hydrogen lean reformate gas in the membrane reactor. For both the activity (modeling) and stability study the Ni-based catalysts were compared to relevant catalyst compositions based on rhodium (Rh). Using the high pressure kinetics reported for Al_2O_3 supported Rh and $MgAl_2O_4$ and Al_2O_3 supported Ni catalyst it showed that Ni and Rh catalysts may very well provide similar hydrogen production rates. Interestingly, the stability of Ni-based catalysts proved to be superior to precious metal based catalysts under exposure to simulated reformate feed gas with low H/C molar ratio. A commercial (pre-)reforming Ni-based catalyst was selected for further testing in an experimental membrane reactor for steam reforming at high pressure. During the test period 98% conversion at 873 K could be achieved. The conversion was adjusted to approximately 90% and stable conversion was obtained during the test period of another 3 weeks. Nonetheless, carbon quantification tests of the Ni catalyst indicated that a small amount of carbon had deposited onto the catalyst. The activity of the Ni catalyst for carbon formation is expected to eventually cause performance loss due to plugging or fouling. Ongoing research efforts are devoted towards the preparation of cost-effective nickel based catalysts with suppressed carbon formation activity.

1. Introduction

Hydrogen membrane reactors are being studied for power production with pre-combustion decarbonisation: the removal of CO_2 from the fossil fuel before combustion takes place. The membrane reactor produces hydrogen used as fuel gas at a low pressure and a steam and CO_2 rich stream at high pressure. Condensation of the steam leaves a concentrated CO_2 stream at high pressure for disposal. In addition, due to the *in situ* removal of reaction products, the reaction equilibriums of the reforming and shift reactions, shown in Eqs. (1)–(3), are shifted to higher conversions (Le Chatelier's principle). Therefore, relatively low temperatures compared to conventional steam methane reforming (SMR) can be used.

$$\text{Steam methane reforming}: CH_4 + H_2O \Leftrightarrow CO + 3H_2 \quad (1)$$

$$CH_4 + 2H_2O = CO_2 + 4H_2 \quad (2)$$

$$\text{Water gas shift}: CO + H_2O \Leftrightarrow CO_2 + H_2 \quad (3)$$

Unlike conventional SMR, membrane reforming benefits from a high operation pressure due to the increased H_2 partial pressure difference across the membrane, which acts as the driving force for hydrogen permeation. The need for multiple shift reaction stages is avoided, and the large wet CO_2 scrubbing section, as is often used for post-combustion capture, becomes much smaller. As a result of the high pressure of the CO_2 stream, the compression requirement is also minimized for the captured CO_2.

Membranes exist that selectively permeate hydrogen between 773 and 873 K with high permeances (in the range of 10^{-6} mol/m^2/s/Pa [1]). Higher temperatures should be avoided due to membrane disintegration risks.

The separated hydrogen will be used as fuel in a gas turbine combined-cycle plant to generate electricity at high efficiency [2]. The implementation of a membrane reactor in a pre-combustion scheme for electricity generation with CO_2 capture is depicted in

* Corresponding author. Tel.: +31 224 568489.
E-mail address: pieterse@ecn.nl (J.A.Z. Pieterse).

0920-5861/$ – see front matter © 2010 Elsevier B.V. All rights reserved.
doi:10.1016/j.cattod.2010.02.032

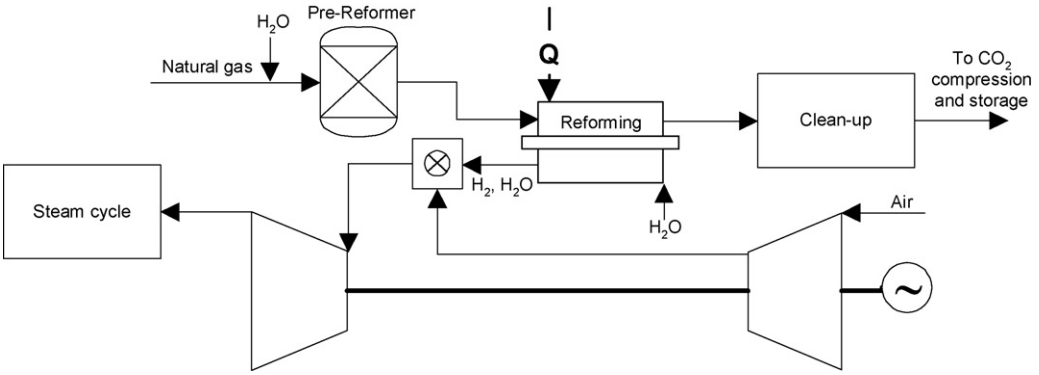

Fig. 1. Power generation with CO_2 capture using a membrane reactor, simplified schematic

Fig. 1. Natural gas first passes a pre-reformer to convert, among others, the heavier parts of the natural gas and trace amounts of sulfur, as well as to increase the partial pressure of hydrogen and preheat the gasses. The reformate then enters the membrane reformer. Hydrogen from the membrane reformer is used in the combustion chamber of the gas turbine. The remaining CO_2 stream is, after clean-up, sent to CO_2 compression and storage. Heat is supplied to the membrane reformer by means of combustion of natural gas or hydrogen (indicated by the Q-arrow). This combustion can occur at atmospheric pressure, or can be integrated with the gas turbine. Flue gas from the gas turbine is used in a steam cycle for generation of steam, which is used for additional power production and for the membrane reactor.

Typically the feed pressure of the membrane reactor equals the pressure at which natural gas is available from high pressure pipelines, i.e. 40–45 bar. Permeate pressure is typically in the range of 5–10 bar. Although the use of the fuel supply pressure of the gas turbine, 17–30 bar, as a permeate pressure would avoid H_2 compression costs, permeation will be significantly hindered.

The requirement for production of a relatively low pressure hydrogen stream for fuel gas and a high pressure CO_2 rich stream for disposal gives obvious scope for the development of membrane reactors. Several gas permeance tests with in-house-made Pd and PdAg membranes show very high hydrogen permeances at sufficient permselectivities [3]. The membranes have been tested for over 100 days on stream using different feed gases and showed stable performances. Nonetheless, the use of a catalyst in membrane reactors poses several challenges. First the activity for both the reforming and water gas shift at relative low temperatures should be sufficiently high. Several precious and base metals show catalytic activity for hydrocarbon steam reforming. It was shown by Rostrup-Nielsen [4] that the turnover frequency-based activity for steam reforming of methane follows the order: Rh, Ru > Ni > Ir, Pd, Pt. Although Rh and Ru are more active than Ni, catalysts used for industrial reforming purposes are most commonly nickel based. After all, Ni is much cheaper than precious metals. Nevertheless, the much lower reaction temperature used in membrane reforming – 873 K while in excess of 1123 K in industrial SMR – may complicate using Ni-based catalyst in membrane reforming. Secondly, resistance to deactivation under the anomalous conditions in membrane reformers is a requisite. High H_2O, CO and CO_2 partial pressures exist in membrane reactors together with low H_2 partial pressure, which may invoke sintering and (sintering-induced) carbon deposition on the catalyst. Moreover, hydrogen withdrawal by permeation also eliminates the thermodynamic restrictions to the formation of carbon. Carbon formation is an established issue in steam reforming catalysis and can cause loss of activity due to blockage of pores, surface fouling and physical decomposition of catalyst support [5]. In steam reforming, carbon could form by methane decomposition and/or Boudouard reaction (CO disproportionation). While high temperatures and low pressures enhance the carbon formation via methane decomposition, this will suppress the carbon formation via the Boudouard reaction. While increasing the total steam content in the feed suppresses carbon formation both thermodynamically as well as kinetically (i.e. by gasification precursors to coke), the use of steam is costly. The steam-to-carbon ratio will, therefore, be limited to 3.

The present study aims at obtaining insight in the potential of nickel based catalysts for steam reforming of methane in membrane reactors. Based on the turnover frequency, nickel catalysts could be less active than precious metal catalysts, yet for an efficient process hydrogen production in the catalyst bed must be sufficiently fast to keep up with the hydrogen withdrawal by the membrane. Therefore, a modelling study was carried out to compare the rate of hydrogen production over nickel and precious metal (PM) based catalysts with the hydrogen flux through a Pd and Pd-alloy membrane. The central question to be answered was whether the Ni-based catalysts are active enough, or that precious metal catalysts are required for faster reaction kinetics. Several in-house-made, pre-commercial and commercial catalysts based on nickel and rhodium have been studied for their methane conversion and stability under conditions that represent the conditions in the membrane reactor already rather well, albeit at atmospheric pressure. From this catalyst evaluation study a promising catalyst was selected and tested in an experimental membrane reactor at high pressure.

2. Experimental

2.1. Membrane reformer modeling

The stipulated arrangement of a tubular membrane with sweep on the inside, and catalyst in an annular zone around the membrane has been simplified to a 1D rectangular geometry, consisting of finite elements (dz) (Fig. 2). Two reactor models have been employed. First, a plug flow reactor model was constructed with hydrogen production from chemical reactions over the catalyst present and hydrogen withdrawal through the membrane. The overall model for the reformer section consists of a system of six coupled differential equations solved in Matlab (ode15s): five equations for the species and an overall material balance for the gas velocity (model 1).

$$\frac{dc_i}{dz} = -\frac{c_i}{u}\frac{du}{dz} + \frac{\rho_b r_i}{u} - \frac{J_i}{d_b u} \quad i = 1,\ldots,5 \quad \text{for} \quad CH_4,\ H_2O,\ CO,\ CO_2,\ H_2 \tag{4}$$

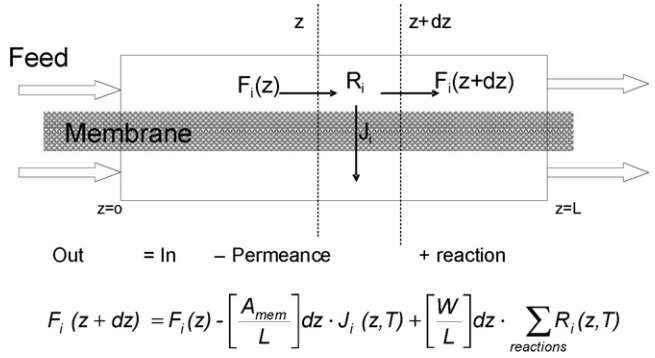

Fig. 2. Simplified model layout of a membrane reformer (model 1). F_i = feed side flux of component i; z = length coordinate; A_{mem} = membrane surface area; L = membrane length; J_i = membrane flux of comp. i; W = catalyst weight; R = reaction rate of comp. I; T = temperature.

$$\frac{du}{dz} = \frac{\rho_b}{c_t}\sum_I r_I - \frac{1}{d_b c_t}\sum_i J_i \tag{5}$$

With c_i the concentration of component i [mol/m^3], z the axial coordinate [m], u the superficial gas velocity [m/s], ρ_b the bed density [kg/m^3], r_i the net reaction rate of component i [mol/kg s], J_i the cross-membrane flux of component i [mol/m^2 s], d_b the catalyst bed width [m], c_t the total concentration [mol/m^3], r_I the net reaction rate for reaction I [mol/kg s]. This first part of the modelling work aimed at comparison of the intrinsic rates of reaction and permeation. The purpose is to test at what effective permeance the expected hydrogen flux through the membrane will be higher than the respective hydrogen production rate on the catalyst, thereby evaluating the required catalyst activity. Any resistance to mass transfer in the catalyst bed, membrane, or permeate is ignored because it would lower the required catalyst activity because it lowers the effective hydrogen flux through the membrane. Only a significant resistance to mass transfer resistance inside the bed (low radial interparticle dispersion) would call for a highly active catalyst in case the permeation is fast enough to deplete the hydrogen near the membrane surface. In such a case, a very active catalyst could be beneficial because it could produce additional hydrogen in the boundary layer near the membrane and thus (partially) counteract the lack of hydrogen transport from the bulk of the catalyst bed. As the model is one-dimensional this effect cannot be taken into account. However, the width of the catalyst bed is kept very small (i.e., 10 mm) so that the resistance to hydrogen transport from the bulk of the catalyst bed may be neglected.

Model 1 is isothermal. This greatly facilitates the modelling, and is not necessarily an unrealistic simplification as a membrane reformer should ideally be operated isothermally. To achieve high fluxes, the operating temperature should be chosen as high as possible. Yet Pd-based membranes are expected to be very sensitive to high temperatures. A maximum operating temperature of 873 K is used, based on experimental data [6].

The rate of hydrogen permeation is calculated from:

$$J_{H_2} = Q_{H_2}(p^n_{H_2,\text{reformate}} - p^n_{H_2,\text{permeate}}) \quad [\text{mol/m}^2\,\text{s}] \tag{6}$$

The permeation rate of all other species is assumed to be negligible. For experimental data describing the hydrogen flux in palladium membranes, the overview by Rothenberger et al. [7] is used. For palladium membranes with a thickness ranging from 0.35 to 244 μm, Rothenberger et al. summarise literature data with n ranging from 0.5 to 1.0. Because a high values of n represents a thin membrane with a high hydrogen permeability, a value of n = 1 has been chosen in this work to maximise the catalytic activity requirement. For this value for n, reported permeances range from $k_{mem} = 5.5 \times 10^{-14}$ to 1.7×10^{-5} mol/m^2 s Pa, with most of the values between 10^{-6} and 10^{-5} mol/m^2 s Pa. Compared to measurements done using pure H_2, in a membrane reformer components such as steam, carbon dioxide, and carbon monoxide could reduce the hydrogen flux, e.g. by introducing mass transfer limitation [8], and co-adsorption on the palladium surface. Catalyst activity was tested with a membrane permeance in the range of 10^{-8} to 10^{-3} mol/m^2 s Pa. The hydrogen partial pressure on the sweep side is set to zero in order to obtain the maximum hydrogen flux.

The rate of chemical reaction is based on kinetic expressions. The reaction equations used are shown in (1)–(3) where (2) is a combination of (1) and (3), and some of the authors only report explicit kinetics for reactions (1) and (3). For ease of calculation and compatibility, the same values for the equilibrium constants are used for all kinetics [9]. The error that is introduced by using general equilibrium constants is accepted as it will not significantly influence the outcome of the calculations.

The sources of kinetics are shown in Table 1, the general forms of the kinetic equations are shown in Table 2. For brevity, the dimensionless parameter β is introduced here, which is defined for reactions (1)–(3) as:

$$\begin{aligned}\beta_1 &= p_{CO}p^3_{H_2}/K_1 p_{CH_4}p_{H_2O}\\ \beta_2 &= p_{CO_2}p^4_{H_2}/K_2 p_{CH_4}p^2_{H_2O}\\ \beta_3 &= p_{CO_2}p_{H_2}/K_3 p_{CO}p_{H_2O}\end{aligned} \tag{7}$$

Note that β = 1 corresponds to a system at thermodynamic equilibrium. As reaction (2) is a combination of (1) and (3) and $\beta_2 = \beta_1 \times \beta_3$, β_2 is used for comparison, representing the overall reaction to CO_2 and H_2. Initially, the gas phase composition is close to equilibrium and high hydrogen partial pressure. This yields low reaction rates and a high membrane flux. Owing to the membrane the hydrogen content of the gas phase will then decrease, increasing the chemical production rate and decreasing the permeation. However, in the largest part of the reformer, the chemical reaction and hydrogen permeation are in equilibrium and the β values have been averaged over the column length for ease of comparison. Prior to use of the Matlab programme it has been checked for errors against reported experimental reaction rates when available [10–13]. Although the reaction conditions used in the studies presented in Table 1 differ to some extend from the membrane reactor system better alternatives are, to our best knowledge, unavailable in literature.

When carrying out the simulations with model 1, a number of additional parameters has to be chosen. The goal is to minimise the membrane surface area, which is commonly considered the most determining factor in costs of a membrane reformer. In an actual application, a pre-reformer or pre-reforming section will be present upstream the actual membrane reformer to increase the hydrogen partial pressure and thus effectively minimising the required membrane surface area. This is also assumed here. The calculation starts with bringing an inlet stream of 25% CH_4 and 75% H_2O to equilibrium at the pressure and temperature of the membrane reformer (all betas equal to one). This result is taken as the inlet of the membrane reformer. The operating pressure and temperature also influence the required membrane surface area. Higher temperatures and pressures increase the flux of hydrogen, and, consequently, it is favorable to operate a membrane reformer close to the maximum feasible operating temperature and pressure. Since membrane lifetime deteriorates quickly at temperatures above 873 K and natural gas from the industrial grid is available at about 40 bar, simulations are carried out at a temperature of 873 K and pressure of 40 bar. The bulk bed density is set at 860 kg catalyst per m^3 reactor. The width of the reforming section in model 1 is arbitrarily set at 10 mm. This value reflects the volume of catalyst

Table 1
Kinetic expressions for methane steam reforming.

	Source	Catalyst	Reactions	Experimental conditions
XF	Xu and Froment [11]	15.2% $Ni/MgAl_2O_4$	(1)–(3)	573–848 K 3–15 bar
NK	Numaguchi and Kikuchi [10]	8.7% Ni/Al_2O_3	(1) and (3)	674–1160 K 1.2–25.5 bar
HH	Hou and Hughes [12]	16% NiO/Al_2O_3 (ICI 57-4)	(1)–(3)	598–823 K 1.2–6.0 bar
WI	Wei and Iglesia [13]	0.1–1.6% Rh/Al_2O_3	(1) and (3)[a]	823–1023 K 1–15 bar

[a] WGS is at equilibrium during experimental measurements. For modelling an arbitrary rate equation is defined ($r = k_3 pCO(1-\beta)$) with the value of k_3 large enough to ensure WGS equilibrium.

Table 2
Kinetic expressions used in the model.

Kinetics	Reaction	Kinetic expression
XF	(1)	$r_1 = \frac{k_1}{p_{H_2}^{2.5}} \left[\frac{\left(p_{CH_4} p_{H_2O} - \frac{p_{H_2}^3 p_{CO}}{K_1} \right)}{\left(1 + K_{CO} p_{CO} + K_{H_2} p_{H_2} + K_{CH_4} p_{CH_4} + K_{H_2O} \frac{p_{H_2O}}{p_{H_2}} \right)^2} \right]$
	(2)	$r_2 = \frac{k_2}{p_{H_2}^{3.5}} \left[\frac{\left(p_{CH_4} p_{H_2O}^2 - \frac{p_{H_2}^4 p_{CO_2}}{K_2} \right)}{\left(1 + K_{CO} p_{CO} + K_{H_2} p_{H_2} + K_{CH_4} p_{CH_4} + K_{H_2O} \frac{p_{H_2O}}{p_{H_2}} \right)^2} \right]$
	(3)	$r_3 = \frac{k_3}{p_{H_2}} \left[\frac{\left(p_{CO} p_{H_2O} - \frac{p_{H_2} p_{CO_2}}{K_3} \right)}{\left(1 + K_{CO} p_{CO} + K_{H_2} p_{H_2} + K_{CH_4} p_{CH_4} + K_{H_2O} \frac{p_{H_2O}}{p_{H_2}} \right)^2} \right]$
NK	(1)	$r_1 = k_1 \frac{p_{CH_4} - p_{CH_4}^{eq}}{p_{H_2O}^{0.596}}$
	(3)	$r_3 = k_3 \left(p_{CO} - p_{CO}^{eq} \right)$
HH	(1)	$r_1 = k_1 \left(\frac{p_{CH_4} p_{H_2O}^{0.5}}{p_{H_2}^{1.25}} \left(1 - \beta_1 \right) / \left(1 + K_{CO} p_{CO} + K_H p_H^{0.5} + K_{CH_4} p_{CH_4} + K_{H_2O} \frac{p_{H_2O}}{p_{H_2}} \right)^2 \right)$
	(2)	$r_2 = k_2 \left(\frac{p_{CH_4} p_{H_2O}}{p_{H_2}^{1.75}} \left(1 - \beta_2 \right) / \left(1 + K_{CO} p_{CO} + K_H p_H^{0.5} + K_{CH_4} p_{CH_4} + K_{H_2O} \frac{p_{H_2O}}{p_{H_2}} \right)^2 \right)$
	(3)	$r_3 = k_3 \left(\frac{p_{CH_4} p_{H_2O}^{0.5}}{p_{H_2}^{0.5}} \left(1 - \beta_3 \right) / \left(1 + K_{CO} p_{CO} + K_H p_H^{0.5} + K_{CH_4} p_{CH_4} + K_{H_2O} \frac{p_{H_2O}}{p_{H_2}} \right)^2 \right)$
WI	(1)	$r_1 = k_1 p_{CH_4} \left(1 - \beta_1 \right)$

per membrane surface area. Therefore a low value requires a high catalyst activity. The value of 10 mm chosen here is a lower limit from practical point of view (reactor loading issues), as a low catalyst volume to membrane surface area ratio puts a higher strain on catalyst activity. The hydrogen permeance k_{mem} was varied in the range of 10^{-8} to 10^{-3} mol/m^2 s Pa. Simulations are stopped as soon as the methane concentration is below 1 mol/m^3, which equals a methane conversion of over 99%. A summary of the simulation input data is provided in Table 3.

In addition to model 1, which was developed solely to compare the intrinsic rate of hydrogen production with representative membrane fluxes, a second model (model 2) was constructed to be able to describe and interpret experimental results. Model 2 matched the experimental conditions in terms of reactor geometry and operating conditions (cf. Section 2.3). A set of 14 coupled

Table 3
Summary of simulation input data (model 1).

Quantity	Value	
$p_{reformate}$	40	bar(a)
$p_{permeate}$	0	bar(a)
T	873	K
$y_{CH_4,in}$	25	%vol of moles
$y_{H_2O,in}$	75	%vol of moles
u_{in}	0.65	m^3/m^2 s
ρ_b	860	kg/m^3
d_b	10	mm
k_{mem}	10^{-8} to 10^{-3}	mol/m^2 s Pa
n	1	

material balances for the reactor and (co-current) sweep side were solved (Matlab ode15s) according to:

$$\frac{dc_i}{dz} = -\frac{c_i}{u}\frac{du}{dz} + \frac{\rho_b r_i}{u} - \frac{J_i}{d_b u} \quad i = 1,\ldots,6 \quad \text{for} \quad CH_4,\ H_2O,\ CO,\ CO_2,\ H_2,\ \text{and}\ N_2\ \text{(reactor side)} \tag{8}$$

$$\frac{du}{dz} = \frac{\rho_b}{c_t}\sum_I r_I - \frac{1}{d_b c_t}\sum_i J_I \tag{9}$$

$$\frac{dc_{i,s}}{dz} = -\frac{c_{i,s}}{u_s}\frac{du_s}{dz} + \frac{J_i}{d_s u_s} \quad i = 1,\ldots,6 \quad \text{for} \quad CH_4,\ H_2O,\ CO,\ CO_2,\ H_2,\ \text{and}\ N_2\ \text{(sweep side)} \tag{10}$$

$$\frac{du_s}{dz} = \frac{1}{d_s c_{t,s}}\sum_i J_i \tag{11}$$

The nomenclature is identical to that of model 1, except for the subscript *s*, referring to sweep side parameters in Eqs. (10) and (11). For each component, the cross-membrane flux is calculated from intrinsic membrane permeance and mass transfer resistance in series:

$$J_i = k_i(c_i - c_{i,s}) \tag{12}$$

With:

$$\frac{1}{k_i} = \frac{\delta}{D_r} + \frac{1}{k_{bnd}} + \frac{1}{Q_i RT} \tag{13}$$

where k_i is the overall mass transfer coefficient (m/s), D_r the interparticle radial dispersion coefficient (m^2/s), δ the respective interparticle radial transport length (m), k_{bnd} the mass transfer coefficient in the boundary layer (m/s), Q_i the membrane permeance for component *i* (mol/m^2 s. Pa), *R* the gas constant (J/mol K), and *T* the temperature (K). Thus, in model 2, mass transfer resistance contributions are incorporated from (1) transport through the bulk of the catalyst bed (δ/D_r), (2) catalyst-membrane film transport ($1/k_{bnd}$), and (3) combined membrane permeation and radial hydrogen transport in the permeate ($1/Q_i RT$). Sweep side (permeate) mass transfer resistance was lumped with the membrane permeation, since these were also measured inseparably. The mass transfer coefficient for laminar film resistance was obtained from literature [14]. Bulk transport was assessed by using a dispersion coefficient from literature [15]. In order to represent an experimentally observed cross-membrane leak, the permeances of all species other than H_2 were set to 1% of the permeance of H_2. The value of δ in model 2 is not estimated a priori but used as a fit parameter. Since the experiments were conducted with a catalyst comprising Ni, Mg and Al (Ni-PR, cf. Section 2.2) the reaction rates were calculated with kinetics as measured for Ni–$MgAl_2O_4$ by Xu and Froment [11].

Both model 1 and model 2 are isothermal. Because of the strongly endothermic steam reforming reactions (1) and (2), this is not a straightforward assumption. Madia et al., for example, predict a significant temperature drop at the membrane reformer inlet due to the high local rates of steam reforming [16]. In spite of their modelling effort, the accurate a priori description of heat transfer in membrane reformers remains a challenge. In membrane reformers, elaborate heat transfer models – based in part on parameters that need to be determined experimentally – such as the Zehner-Bauer model are required for heat transfer modelling, since the contribution of the static thermal conductivity of the bed (i.e., in absence of flow) will probably be significant [15, Section IX.2.2]. In addition, accurate measurement of temperature distributions in relatively small-scale membrane reformers is not at all straightforward. Nevertheless, the anticipated temperature effect is expected to be significant for the very reactor inlet only [16]. Only at this point are the local rates of steam reforming high enough to cause a significant temperature dip. In the current experimental configuration, as well as in model 2, this occurs in a pre-reformer section only: in the first 4 cm of the catalyst bed there is no membrane. Predicted reaction rates with model 2 show that the high reaction rates are expected only in less than 1 cm from the reactor inlet; similarly, the modelling by Madia et al. predicts a temperature dip that extends for roughly the first 4 cm only. In conclusion, any temperature effects will likely be located in the first part of the reactor only, where there is not yet a membrane in our configuration. Any temperature effect will therefore neither affect the outcome of experiments, nor the modelling work.

Table 4
Catalysts used in the stability study.

Catalyst code	Support	Ni (wt%)	Dispersion (%)	Rh (wt%)
18NiMA	$MgAl_2O_4$	19.1	4.3	–
40NiMA	$MgAl_2O_4$	40.4	n.a.	–
20NiMA HDP	$MgAl_2O_4$	19.2	6.1	–
05Rh-MA	$MgAl_2O_4$	–	n.a.	0.5
Ni-PR	n.a.	n.a.	n.a.	–
PM-SR	n.a.	n.a.	n.a.	n.a.

n.a., not analyzed.

2.2. Catalyst and membrane preparation

Nickel based and precious metal based catalysts were obtained from catalyst vendors. Besides, several nickel based catalyst were synthesized. Nickel was loaded by incipient-wetness impregnation or homogeneous deposition precipitation (HDP) of $MgAl_2O_4$ (MkNano) support. For impregnation, typically the $MgAl_2O_4$ was treated with a solution of the nitrate-salt of nickel (87.34 g $Ni(NO_3)_2{\cdot}6H_2O$ was dissolved in 35 g of demiwater) equal to the pore-volume of the support material (0.7 ml/g). Nickel loadings were chosen 19.1 and 40.4 wt% and confirmed by EDX analysis (the average wt% of 16 independent scans on 4 different locations).

For the homogeneous deposition precipitation, the nickel is precipitated on the support following the procedure given by Geus and Van Dillen [17]. 1 g of $MgAl_2O_4$ was mixed in a large amount of water (150 ml). Nickel salt 1.6514 g was then added (pH ≈ 7–9). The pH was brought to 2 with a HNO_3 1 M solution. The suspension was stirred and heated at 90 °C for the precipitation. The aqueous solution of urea (1.2312 g urea dissolved in 20 ml) was added. The mixture was cooled down and filtrated after 16 h. Table 4 provides an overview of the catalysts used in this study.

The catalysts were dried at 353 K overnight. Dried samples were then calcined (under air) in a tube oven at 898 K for 5 h. Prior to catalytic testing, the catalysts were reduced *in situ* with a ramp-up of 1.2°K/min to 573 K under 5% H_2 in N_2 and then heated with 1.2°K/min to 873 K under 34% H_2 in N_2 with 5 h dwell time at 873 K. For membrane preparation first a commercial α-Al_2O_3 macroporous membrane support tube (Tami) was tailored by suspension film coating two additional microporous 45 μm α-Al_2O_3 layers [18]. Then a thin Pd layer with a thickness of 3.8 μm was applied by electroless plating [19]. The membrane was fitted with proprietary metal–graphite compression sealings [20]. The leak tightness of the membrane with a surface area of 155 cm^2 was checked with separate N_2 and hydrogen feed flows together with the stability of the H_2 flux during the course of the experiment.

2.3. Catalyst testing and characterization

Reforming experiments were performed with microflow reactors, in setups containing one or six quartz reactors in parallel. Catalyst stability testing was conducted at 773 and 873 K. Gas compositions varied from 7.5% CH_4, 22.5% H_2O, 5% Ar balance N_2 (denoted reference condition, "REF", representing conventional steam methane reforming) to 1.3% CH_4, 3% H_2, 16% H_2O, 0.14% CO, 11.8% CO_2, 5% Ar, balance N_2. The latter condition is denoted membrane condition (MR). The specific concentration of the gas components in the MR condition is obtained on the basis of thermodynamic calculations of equilibrium gas compositions (using Outokumpu Research's HSC Chemistry version 5.1) after reforming a 7.5% CH_4, 22.5% H_2O feed. From the thermodynamic equilibrium composition, H_2 is removed in order to simulate the membrane effect. The resulting gas mixture after H_2 removal is input for the next equilibrium calculation. This procedure is carried on until the gas composition corresponding with a desired CH_4 conversion is reached, e.g. 91%. Doing this, the hydrogen concentration in the MR condition should be 1%: the hydrogen is however set to 3% H_2 in the MR condition as this turned out to be the minimum setpoint to allow accurate hydrogen dosing by the mass flow controller. By switching the REF condition to the MR condition the molar ratio of hydrogen to carbon, i.e. H/C, decreases from 10 to 2.9 (at a constant O/C of 3). The approach of Kleinert et al. [21] is to mimic membrane reforming conditions with variation of H_2O/CH_4 ratio. In the present study we favor the comparison of H/C ratio's rather than steam/methane ratio's. Using the simulated membrane condition we manage to compare significantly different H/C ratio's while leaving the O/C ratio constant. The effect of the membrane is to remove H only. As such the study of various methane/steam ratio's does not fully reflect steam reforming in the presence of a membrane.

Gas chromatography (CompactGC, Interscience BV) and NDIR (non-dispersive IR, ABB) was used for analysis of the dry gas samples.

Temperature programmed reduction (TPR) and oxidation (TPO) was carried out using an Altamira AMI-200 apparatus, equipped with TCD and a calibrated Balzers Quadrustar mass spectrometer to allow for quantification of hydrogen uptake during reduction or chemisorption and CO_2 formation (carbon) during TPO. During TPO (ramp rate 10 K/min), from 303 to 1273 K, carbon (C) desorbs from the catalyst surface while being oxidized, forming CO_2. Prior to TPO, the sample was evacuated for 2 h at 373 K under a stream of argon. The mass spectrometer was calibrated by pulsing of 522 μl of CO_2 and recording the $m/e = 44$ mass fragment intensity with a quadrupole mass spectrometer. This procedure was repeated 15 times and the average integrated area was used in the calculations (standard deviation < 1%). The CO_2 evolution peaks formed during TPO were integrated over time and the amount of C was quantified. The TPO was carried out in triplicate. Similarly, TPR was measured by raising the temperature at a rate 10 K/min, from 303 to 1273 K in hydrogen.

The same setup was also used to determine CO-uptake of the nickel catalyst. This analysis allowed to compare dispersion of the active Ni phase with deposition precipitation and impregnation synthesized catalysts. The catalysts were reduced at 923 K in 30% H_2, evacuated in Ar atmosphere by cooling down to 323 K. Subsequently, CO was pulsed with pulses of 59 μl until saturation was obtained. In order to validate the results of the quantification of carbon by TPO and TPR CHNS analysis was conducted with a CHNS analyzer (Thermo Scientific FLASH 2000).

A Renishaw inVia Raman microscope system was used for RAMAN measurements. The system contains a set of objectives (5×, 20× and 50×), monochromators, a filter system and a charge coupled device (CCD). Raman spectra were excited by a He–Ne laser (522 nm) in the range between 100 and 3200 cm^{-1}.

2.4. Membrane reactor testing

A high pressure, high temperature facility for testing under realistic process conditions (feed pressures up to 64 bar, temperatures up to 973 K) has been used for membrane reactor tests (see Fig. 3). The facility contains a one-tube membrane reactor (module, see Fig. 4). The feed is fed on the outside of a membrane with a length of 35.1 cm and area of 155 cm^2. The catalyst is placed between the outside of the tubular membrane and inside of the metal tube in which the membrane is placed. Sweep is introduced through an

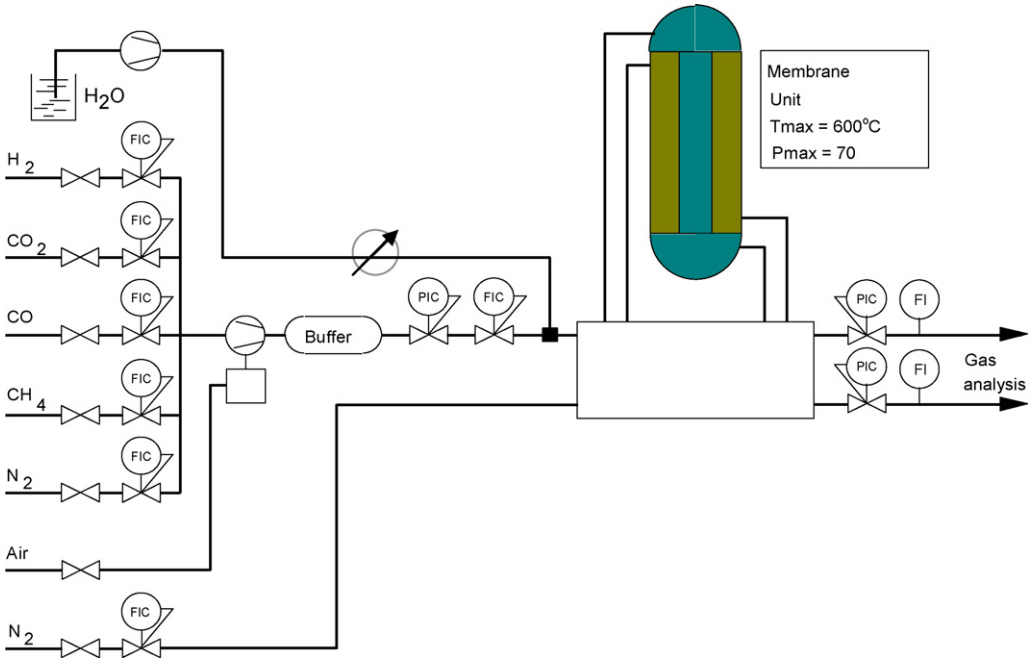

Fig. 3. Simplified flowsheet of the high pressure gas separation equipment.

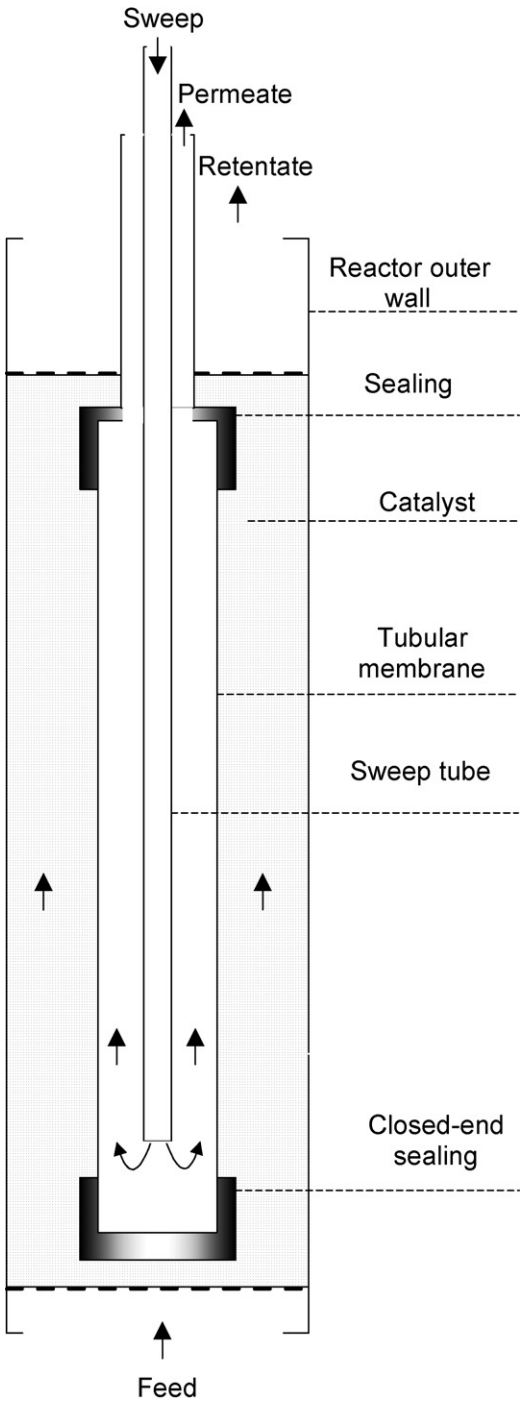

Fig. 4. Schematic of tubular membrane reactor arrangement.

insert tube and in co-current mode to avoid back-permeation of hydrogen from the permeate side to the feed side. The module is placed in an oven that can be heated to a maximum temperature of 973 K. The feed line is passed through the oven to pre-heat the feed stream prior to entering the membrane module. Next to the oven temperature, the catalyst temperature was measured at the reactor entrance and outlet.

Feed and sweep gasses are supplied through mass flow controllers. Retentate and permeate compositions are analyzed with a Varian 3600 gas chromatograph.

The membrane reactor experiments have been performed with a nitrogen diluted reformer feed mixture with a steam-to-carbon ratio of 3 at 823 and 873 K. First the performance of the membrane reactor was studied at different feed pressures, feed flows and nitrogen dilution. After 10 days the membrane reactor was operated at constant conditions for 40 days. The catalyst used was Ni-PR.

Table 5a
General conditions of the membrane reactor testing.

	Test 2
$T_{reactor}$ (K)	803–863
P_{feed} (bar(a))	25–42
CH_4/H_2O feed	1:3
$p_{permeate}$ (bar(a))	1.0
Membrane type	Pd/Al_2O_3
Membrane layer thickness	3.8 μm
Membrane length/diameter (cm)	35.1/1.4
Reactor diameter cm	2.6 cm
Catalyst type	Ni-PR
Catalyst mass (g)	195
Catalyst strainer fraction (mm)	0.8–1.2 mm

The conditions of the membrane reactor testing are compiled in Tables 5a and 5b. Single gas hydrogen permeance was measured prior to and after the membrane reactor test with catalyst inside.

3. Results and discussion

3.1. Theoretical evaluation of the required catalyst activity in the membrane reformer

In order to determine the minimum activity necessary to keep membrane flux rate determining and to obtain insight in the question whether Ni-based catalysts active enough model 1 was used as described in Section 2.1. Fig. 5 shows the results of the model at P_{feed} 40 bar, $T = 873$ K and diameter of the catalyst bed $H = 10$ mm. As the membrane permeance k_{mem} is increased, all catalysts reach a point where they are no longer able to maintain chemical equilibrium (length averaged $\beta < 1$). At this point, the removal of hydrogen by the membrane is faster then the hydrogen generation through the combined reforming reactions. For the Ni-based catalysts, there is a significant spread in activity among the studies. Numaguchi [10] predicts the lowest activity rates, while Xu [11] predicts the highest. The relatively low activity of the Numaguchi kinetics could be linked to the lower Ni content and to the fact that they make use of γ-Al_2O_3 support, which is known to give $NiAl_2O_4$ spinel with decreased activity during reductive activation [22]. This also explains why Hou [12] predicts a lower activity than Xu, respectively using γ-Al_2O_3 and $MgAl_2O_4$ support. Interestingly, the

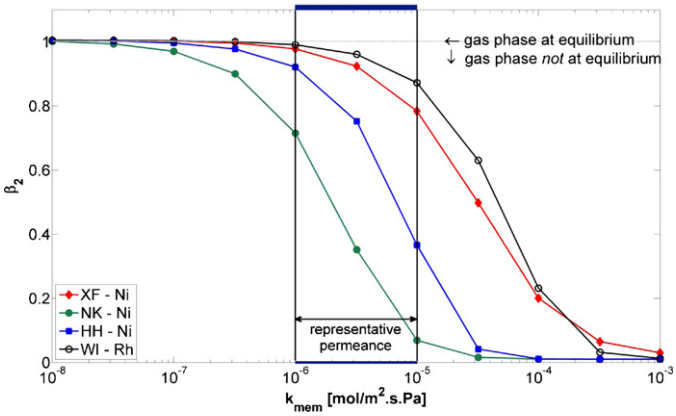

Fig. 5. Length averaged β-values for reaction (2) versus membrane permeance for different kinetics (40 bar, 873 K, $d_b = 10$ mm).

Table 5b
Detailed conditions of the membrane reactor testing.

Exp	$p_{retentate}$ [bar(a)]	$p_{permeate}$ [bar(a)]	$T_{membrane}$ [K]	Feed			Sweep
				N_2 (mol/s)	CH_4 (mol/s)	H_2O (mol/s)	N_2, sweep (mol/s)
MR1	27.30	1.00	840	7.3E−04	1.8E−04	6.2E−04	4.3E−05
MR2	33.10	1.00	851	7.4E−04	1.8E−04	6.1E−04	4.3E−05
MR3	25.40	1.00	820.6	1.8E−03	5.8E−04	1.7E−03	4.3E−05
MR4	35.30	1.10	834.4	1.7E−03	7.0E−04	1.7E−03	4.3E−05
MR5	27.60	1.00	853.3	2.4E−03	1.3E−04	1.7E−03	4.3E−05
MR6	41.80	1.00	860.6	2.4E−03	1.3E−04	1.7E−03	4.3E−05
MR7	24.10	1.00	824.1	1.7E−03	5.9E−04	1.7E−03	4.3E−05
MR8	24.50	1.00	836.6	1.7E−03	5.8E−04	1.7E−03	4.3E−05
MR9	24.10	1.00	821.6	1.7E−03	5.8E−04	1.7E−03	4.3E−05
MR10	24.50	1.00	814.5	1.7E−03	5.9E−04	1.7E−03	4.2E−05
MR11	24.50	1.00	828.6	1.8E−03	5.7E−04	1.7E−03	4.3E−05
MR12	25.90	1.00	818.7	1.9E−03	5.9E−04	1.7E−03	4.2E−05
MR13	24.40	1.00	822.1	1.8E−03	5.8E−04	1.7E−03	4.2E−05
MR14	25.90	1.00	821.3	1.8E−03	5.8E−04	1.7E−03	4.3E−05
MR15	26.10	1.00	822.1	1.8E−03	5.8E−04	1.7E−03	4.2E−05
MR16	26.10	1.00	816.3	1.8E−03	5.8E−04	1.7E−03	4.2E−05
MR17	26.10	1.00	821.3	1.8E−03	5.8E−04	1.7E−03	4.4E−05
MR18	26.10	1.00	812.2	1.8E−03	5.8E−04	1.7E−03	4.3E−05
MR19	26.30	1.00	823.8	1.8E−03	5.8E−04	1.7E−03	4.3E−05
MR20	26.10	1.00	820.8	1.8E−03	5.8E−04	1.7E−03	4.3E−05
MR21	26.80	1.00	825.4	1.8E−03	5.8E−04	1.7E−03	4.3E−05
MR22	25.70	1.00	829.8	1.8E−03	5.8E−04	1.7E−03	4.4E−05
MR23	26.70	1.00	836.4	1.8E−03	5.8E−04	1.7E−03	4.4E−05
MR24	25.60	1.00	830	1.8E−03	5.8E−04	1.7E−03	4.4E−05
MR25	26.10	1.00	829.8	1.8E−03	5.8E−04	1.7E−03	4.4E−05
MR26	25.70	1.00	833.3	1.8E−03	5.8E−04	1.7E−03	4.4E−05
MR27	25.30	1.00	835.5	1.8E−03	5.8E−04	1.7E−03	4.4E−05
MR28	25.50	1.00	820.3	1.8E−03	5.8E−04	1.7E−03	4.4E−05
MR29	26.10	1.00	835.5	1.8E−03	5.8E−04	1.7E−03	4.4E−05
MR30	25.60	1.00	838.6	1.8E−03	5.8E−04	1.7E−03	4.4E−05
MR31	25.30	1.00	840.8	1.8E−03	5.8E−04	1.7E−03	4.4E−05
MR32	25.20	1.00	842.4	1.8E−03	5.8E−04	1.7E−03	4.4E−05
MR33	24.70	1.00	828.8	1.8E−03	5.8E−04	1.7E−03	4.4E−05
MR34	24.80	1.00	836.8	1.8E−03	5.8E−04	1.7E−03	4.4E−05
MR35	24.80	1.00	830.7	1.1E−03	3.5E−04	1.7E−03	4.7E−05

kinetics of Xu (nickel) predicts an activity similar to that of Wei (rhodium) [13]; both maintain equilibrium conversion at a representative high permeance of 10^{-6} mol/m^2 s Pa.

Severe simplifications were made in model 1. Firstly, the hydrogen permeance used is an effective one incorporating mass transfer effects and surface adsorption effects on the membrane surface. These should not be compared to permeances obtained in pure gas experiments, but rather to the apparent permeance obtained in real-application experiments. Transport resistances between catalyst and membrane will decrease the required catalyst activity at a certain permeance, which implies that in realistic systems it will be easier to maintain thermodynamic equilibrium compared to the calculations. Shown in Fig. 5, the activity as predicted by Xu and Froment kinetics for a nickel catalyst would be sufficient under the right operating conditions, i.e. an apparent permeance equal to or below 10^{-5} mol/m^2 s Pa. In such a case, the gas phase composition in the catalyst bed is still close to chemical equilibrium and the hydrogen production rate on the catalyst is sufficiently high to balance the hydrogen flux through the membrane. All in all, nickel based catalysts should not be dismissed based on their activity for membrane reforming applications.

The simplification to a one-dimensional model implies that important effects of mass transfer (concentration gradients in the radial direction) and heat transfer (temperature gradients in the radial direction) are not fully accounted for. Future work on two-dimensional modeling of membrane reactors should determine whether these effects make the demands to catalyst activity higher (only part of the catalyst bed is used due to mass and heat transfer limitations) or less (e.g. high temperatures and off-equilibrium concentrations boost hydrogen formation).

3.2. Catalyst stability under simulated membrane reforming conditions

Fig. 6 shows the methane steam reforming conversion as a function of the time-on-stream for two precious metal based catalysts. PM-SR is a commercially available precious metal catalyst for steam reforming, 05Rh-MA is in-house-made 0.5 wt% Rh supported by $MgAl_2O_4$. Because the metal loading of PM-SR is unknown the ini-

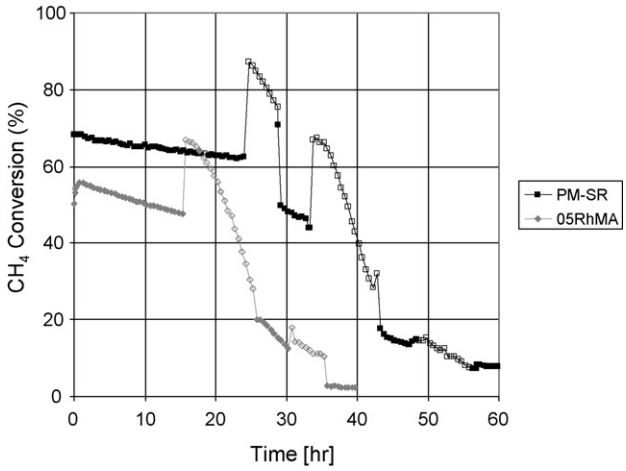

Fig. 6. Methane steam reforming conversion with supported PM catalysts during two interchanging conditions REF and MR. The open marker symbols represents data collected while the catalyst was operated under MR conditions.

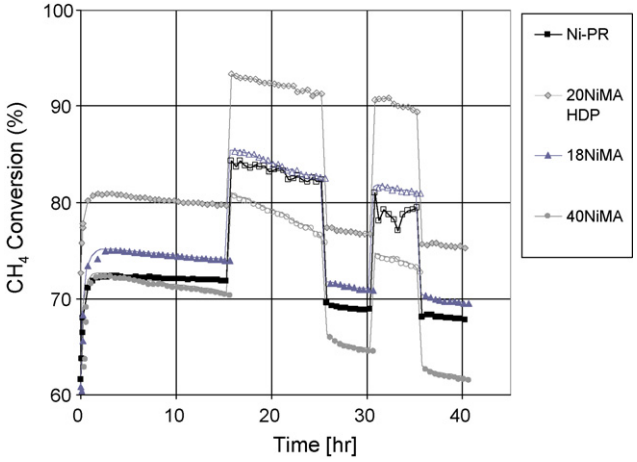

Fig. 7. Methane steam reforming conversion with supported Ni catalysts during two interchanging conditions REF and MR. The open marker symbols represents data collected while the catalyst was operated under MR conditions.

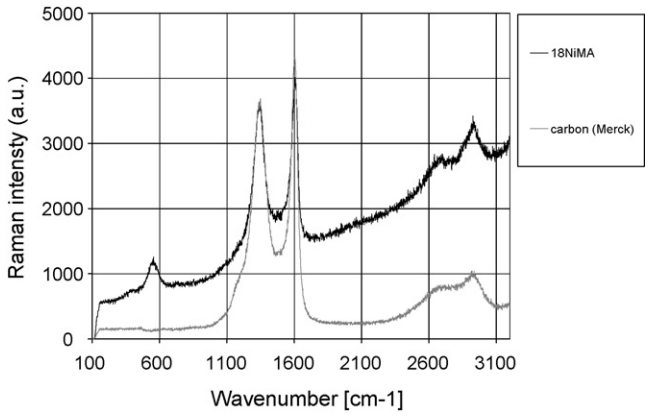

Fig. 8. Raman spectra of 18NiMA used in reaction and reference carbon obtained from Merck.

tial activities cannot be compared directly in terms of turnover frequency. To separate true deactivation from decreased reaction rates due to approach to equilibrium, a low β is mandatory for all reactions involved (1)–(3) [13]. The beta for the second or overall reaction (β_2) during the testing was kept below 0.10 during all experiments. The catalysts have been diluted with inert alumina (1:19) in order to ensure that the conversion level is far from equilibrium conversion. Both catalysts deactivate to some extent during the first reference condition, the commercial catalyst somewhat less severely. Upon exposure to the membrane feed composition, the immediate onset of rapid deactivation is noticed. Also the extent of deactivation during the subsequent second REF condition became much higher than expected from the trend obtained during the first REF period.

The extent of deactivation of Ni catalysts show similarities to the trends observed for the PM based catalysts for the very first REF sequence, see Fig. 7. Interestingly, the deactivation is only marginally affected by the MR conditions contrary to the case with the PM catalysts. The highly loaded Ni catalyst reveals the most significant deactivation. Homogeneous deposition precipitation Ni catalyst gives somewhat more stable reforming performance compared to impregnated Ni catalyst. This is presumed to relate to the small Ni particles formed by HDP method, which are less susceptible to carbon formation [17]. Comparing the slopes of the deactivation during the REF (see Table 6, slopes denoted kd (h^{-1}) for RC1, 2, 3: the "1", "2" and "3" refer to the first, second and third time the feed was adjusted to reference condition during the course of the stability testing) and MR sequences it follows that the HDP prepared catalyst and the commercial Ni-PR catalysts show identical moderate deactivation. Given its availability and relatively good performance the commercial Ni-PR (nickel pre-reforming) catalyst was selected for further membrane reactor testing.

Table 6
Slopes of the deactivation during three REF conditions.

Catalyst	kd (h^{-1})		
	RC1	RC2	RC3
18NiMA	−0.09	−0.16	−0.17
40NiMA	−0.15	−0.26	−0.27
20NiMA HDP	−0.07	−0.14	−0.09
Ni-PR	−0.04	−0.16	−0.12

The fresh reduced 18NiMA catalyst showed a dispersion of approximately 4%, which is within the range of dispersion values for nickel catalysts with high loadings [4]. Due to the large Ni particle size and the highly diluted state of catalysts the low CO-uptake did not allow for a quantitative analysis. CO-uptake does however allow for a qualitative evaluation of the particle size of Ni catalysts prepared by different synthesis methods. As followed from the CO-uptake, the particle size of the impregnated catalyst was found approximately 30% higher than for the HDP synthesized catalyst with the same Ni loading (Table 4).

Deactivation of Ni catalysts may be caused by carbon formation, oxidation during reaction and sintering (which in turn may boost structure sensitive carbon deposits to be formed). The contribution of sintering could not be investigated for the reasons of the limited quantitative value of CO chemisorption. A role for Ni oxidation to catalyst deactivation was studied as follows: First the calcined Ni catalyst 18NiMA was reduced at 873 K for 5 h after which the oxygen consumption was determined during subsequent TPO. Using the stoichiometry of $2NiO \Rightarrow 2Ni + O_2$, together with the Ni loading, the amount of non-reduced Ni after reduction at 873 K for 5 h was determined to be approximately 10%. Incompleteness of the reduction of MgO supported NiO is reported before [4]. Secondly, new batches of calcined Ni catalyst 18NiMA were treated in exactly the same manner except for a new treatment procedure in between the TPR and TPO. The new treatment procedure consisted of exposing the catalyst to a mixture of $H_2O/H_2/N_2$, molar ratios 9/1/1 and 9/0/1 during 50 h on stream in two independent measurements. Even after H_2O/N_2 exposure at 873 K (without H_2) the extent of re-oxidation was in the order of only $2 \pm 1\%$. Therefore, the oxidation of Ni during steam reforming is not believed to be significant and extended research to the cause of deactivation was focused on carbon formation. It is worth mentioning that thermodynamic analysis with HSC software does not predict re-oxidation at 873 K and the feed compositions used for catalyst testing.

RAMAN studies showed that the deactivated catalysts have carbon deposits with similarities to the polycrystalline graphite in the reference active carbon material (Merck) (see Fig. 8). The peak at approximately 550 cm^{-1} is due to some NiO in accordance with the aforementioned incomplete reduction of Ni at 873 K. Carbon analysis was further elaborated on using catalyst samples obtained from the membrane reactor module after extended periods of SRMR testing and is discussed in Section 3.3.

3.3. Membrane reactor testing (SRMR)

The principle of increased CH_4 conversion in low temperature steam methane reforming (SMR) with a reactor containing a H_2

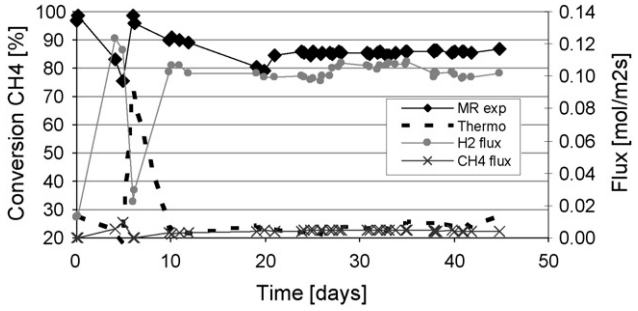

Fig. 9. Methane conversion as a function of the time-on-stream in the membrane reactor (P_{feed} = 25–42 bar(a), CH_4/H_2O = 1/3, T = 803–863 K).

selective Pd membrane was studied with the membrane reactor module as described in Section 2.4. Special attention was also given to the stability of the membrane reforming process during extended periods on stream. Finally the membrane reactor model 2 results have been compared with the experimental data.

Fig. 9 shows both the methane conversion and methane and hydrogen fluxes as a function of the time-on-stream. As shown in Fig. 9 near complete conversion of methane could be obtained during experiments with varying combinations of flows and pressures that were performed during the first 10 days. The H_2 flux of the unit was dependent on MSR feed flow rate. After 5 days of operation, and again after 10 days of operation, the hydrocarbon feed flow was increased, resulting in increases in the H_2 flux and slight decreases in conversion, i.e. 87% methane conversion. During the subsequent testing period of another 41 days a steady conversion of close to 90% was obtained. Note that the equilibrium conversion without hydrogen permeation is at these condition is in the range of 15% (feed composition mol% N_2 48, H_2O 40, CH_4 12, T = 856 K, P_{feed} = 27.5 bar).

Fig. 10 shows the hydrogen recovery and the hydrogen concentration during the membrane steam reforming run. The performance of the membrane (Figs. 9 and 10) was stable over the fixed operation period. Using a constant small nitrogen sweep flow the hydrogen purity decreased during the first 10 days (loss of H_2/N_2 permselectivity) towards a stable hydrogen purity between 80 and 90 mol% during the stability testing at a stable hydrogen recovery of 70%. The hydrogen flux was dependent on the feed flow rate and the operating pressure. At day 4 the methane feed was increased, resulting in an increase in the H_2 flux and a decrease in conversion. When operating conditions were held constant the H_2 flux and conversion were very stable. The highest hydrogen flux demonstrated for this trial was 0.12 mol/m^2 s and conversions varied between 98 and 75%. The retentate stream from the reactor, measured at maximum H_2 flux contained, after subtracting the

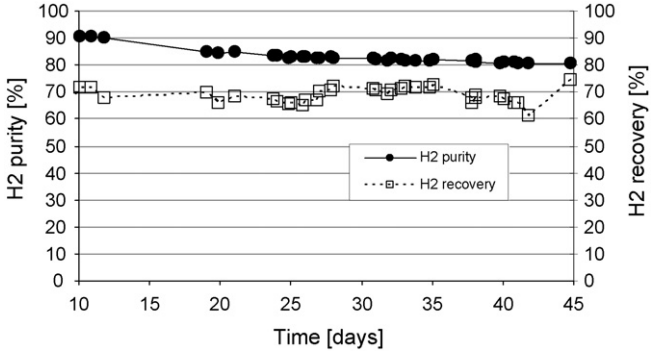

Fig. 10. Hydrogen recovery and purity as a function of the time-on-stream in the membrane reactor (863 K, Pf 29 bar(a) N_2 sweep 0.05 ml/min, CH_4/H_2O = 1/3).

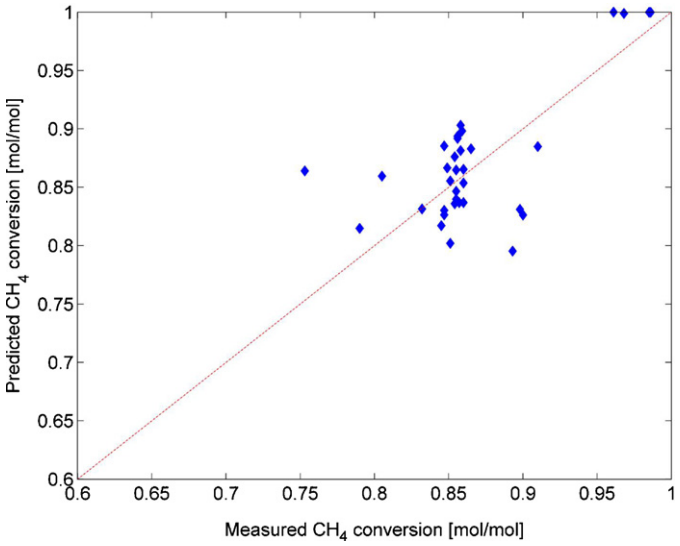

Fig. 11. Methane conversion as predicted by the model (model 2) versus experimentally observed methane conversion.

nitrogen dilution, 90 mol% CO_2 and 0.7 mol% CO (dry basis). Single gas permeation tests prior and after the membrane reactor test show a decrease in H_2/N_2 permselectivity from 1764 to 47.1 at 36–41 bar feed pressure, which is probably the reason for the small decline in permeate purity. The H_2 single gas permeance was at the start of the membrane reactor tests 4 mmol/m^2 s Pa$^{0.5}$ at 796 K and afterwards 4.6 mmol/m^2 s Pa$^{0.5}$ at 870 K.

The results of the membrane reactor experiment (Figs. 9 and 10) were used to validate model 2. However, in order to assess the mass transfer due to radial dispersion, the transport distance for radial dispersion needs to be known. The transport distance of hydrogen through the bulk was, therefore, fitted to the experimental results using transport distance delta (δ): δ = 0 means a very active catalyst that produces sufficient hydrogen immediately at the interface catalyst bed-membrane. Experimental results could by reproduced with a value of δ = 0.31 mm. Combined measurement of the permeance and radial permeate transport resistance in pure gas H_2 permeation measurements at 796 and 870 K lead to a hydrogen permeance of

$$Q_{H_2} = 4.08 \times 10^{-5}\ \text{mol/m}^2\ \text{s Pa} \times \exp\left(\frac{-16.4\ \text{kJ/mol K}}{RT}\right) \qquad (14)$$

To compensate for a reduction in the effective permeance by co-adsorption of CO, CO_2, and H_2O [8,23–25], the pure hydrogen permeance was multiplied by 0.6. To incorporate a small leak flow (as observed in the experiment) the permeance of all other components was set to 1% of the respective hydrogen permeance. Using co-current operation with values for feed flow, sweep flow, feed and permeate pressure in accordance with the experiment, the experimentally obtained methane conversion was reproduced (with δ = 0.31 mm as fit parameter). The comparison to the experimental and model results is given in Fig. 11.

While these tests indicate that stable conversion in SRMR can be achieved with Ni-PR catalyst some catalyst deactivation related to carbon deposition may be envisioned from the tests at low pressure described in Section 3.2. Carbon formation is a structure sensitive process. High steam partial pressure in the membrane reactor may cause sintering of the nickel particles, which in turn are more susceptible to carbon deposition. It should be noted that in the current SRMR tests the catalyst deactivation may be significant although invisible: catalyst volume used may be significantly overdimensioned in relation to the minimum hydrogen production rate required to ensure hydrogen permeance to be rate limiting.

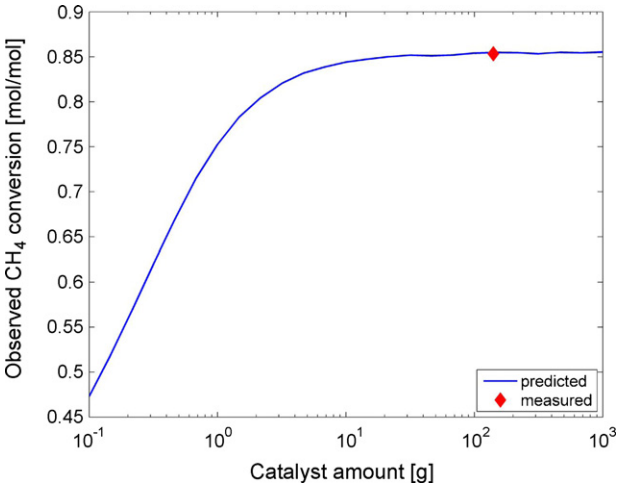

Fig. 12. Effect of the amount of catalyst in the membrane reformer on the observed methane conversion as predicted by the 1D model with mass transfer limitations (model 2) (–) and the measured average methane conversion in the duration test (♦).

Using model 2, an estimate was made of the effect of catalyst deactivation upon the overall methane conversion. The purpose of this work was to establish whether or not the observed stability in methane conversion (cf. Fig. 9) also points to a stable catalyst activity, or rather that a decay in catalyst activity is disguised by an excess of catalyst in the reactor. The parameters in the model were fixed to the values of the duration test (days 11–45 in Fig. 9) and the amount of catalyst in the model was varied to reveal the effect of catalyst activity on the apparent methane conversion. Fig. 12 shows the result of the calculations. Here the methane conversion with 195 g of catalyst (original experiment) is compared to the observed methane conversion with a reduced amount of catalyst as estimated by the model. Clearly, deactivation of the catalyst does not directly result in a lower observed methane conversion because the catalyst is not limiting the conversion. The observed stability (Fig. 9) therefore does not imply that the reforming catalyst was actually stable during the test. The minimum amount of catalysts to operate the membrane reactor module used in this study is estimated a factor 1.5–2 orders of magnitude lower than the amount of catalyst used in the experiment shown in Fig. 9.

Characterization of the carbon deposits on the catalyst after the test period shown in Fig. 9 confirmed that carbon had formed during SRMR. Temperature programmed oxidation and reduction studies on Ni-PR catalyst were carried out to quantify the amount of carbon deposited during reaction. Both methodologies were checked for their ability to account for all carbon by comparing the results with CHNS results. After the reaction in the membrane module the catalysts was first separated in the top fraction (the first 14 cm of the catalyst bed), middle fraction and the bottom fraction, i.e. the fraction gathered in the last 14 cm of the reactor. The results of the carbon analysis are shown in Table 7. CHNS indicated 1–1.3 wt% carbon, without a clear difference between top, middle and bottom location. TPO quantification gave similar results although some part of the carbon was trapped into CO (visualized by an *m*/*e* 28 peak at approximately 623 K) instead of CO_2: this CO was not accounted for

Table 7
Carbon quantification after SRMR.

	CHNS (wt% C)	TPO (wt% C)	TPR (wt% C)	CHNS after TPR (wt% C)
Top	1.1	1.2	0.2	0.7
Middle	1.3	0.7	0.3	n.a.
Bottom	1.2	1.5	0.3	0.8

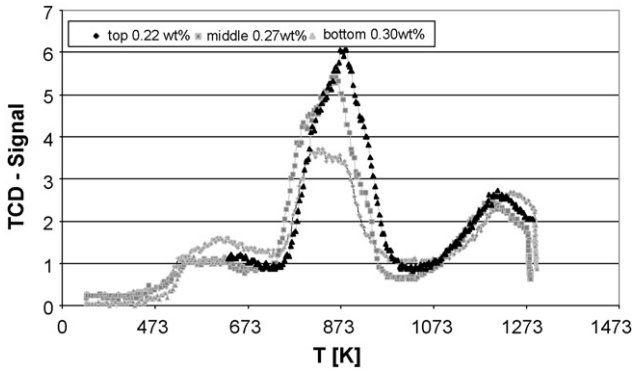

Fig. 13. TPR of the catalyst used in the SRMR testing.

in the quantification. Clearly, TPR analysis did not account for all the carbon. Nevertheless, TPR allows for assigning various types of carbon according to McCarty et al. [26]. McCarty et al. have devised a classification of the types of coke that are formed on nickel reforming catalysts that has been widely adopted in ensuing publications on the subject. The catalyst samples are heated with a constant rate from room temperature to about 1273 K in hydrogen. During the process, carbonaceous species are reduced to methane at a temperature that is indicative of the type of species involved. Either the hydrogen consumption or the methane production can be plotted against temperature, showing peaks that are characteristic of the types of carbon on the sample.

Fig. 13 gives an example of the TPR spectrum of the Ni-PR catalyst after the 4 weeks testing in the membrane reactor module. Peaks are observed at approximately 573, 873 and 1173 K representing some chemisorbed carbon, gum-like carbon structure and carbon with graphitic structure, respectively. The fresh catalyst did not have any significant amount of carbon (not shown). The catalyst section was significantly over-dimensioned and catalyst deactivation could not be visualized within the time-span of the experiment. At the same time the quantification of the carbon described is somewhat underestimated by dilution of catalyst with relative fresh, non-used catalyst fractions. To summarize, carbon formation will sooner or later cause performance loss of SRMR and catalyst design should be custom-tailored toward blocking of carbon formation pathways.

4. Conclusions

The activity of nickel catalysts in SRMR was assessed with kinetics reported in literature and a 1D model was composed to compare hydrogen production rates with the rate of hydrogen deprival by permeation. Using the high pressure kinetics reported for alumina supported rhodium and $MgAl_2O_4$ supported nickel it showed that nickel and rhodium catalysts may very well provide similar hydrogen production rates. As the membrane permeance is increased, all catalysts reach a point where they are no longer able to maintain chemical equilibrium. However, for permeances representative for state-of-the-art Pd-alloy membranes, both types of catalysts appear to provide sufficient activity. The stability of nickel based catalysts proved to be superior to precious metal based catalysts under exposure to simulated reformate feed gas with low H/C molar ratio. A Ni-based catalyst was therefore selected for further testing in an experimental membrane reactor for steam reforming at high pressure. During the test period 98% conversion at 873 K could be achieved. The conversion was adjusted to approximately 90% and stable conversion was obtained during the test period of another 3 weeks. Nonetheless, carbon quantification tests of the Ni catalyst used in typical SRMR tests indicate that a

small amount of carbon deposited onto the catalyst. Supplementary reactor modelling showed that the catalyst bed is likely to be over-dimensioned and that even significant catalyst deactivation may not be observed in the membrane reactor test. The substantial activity of the Ni catalyst for carbon formation is expected to eventually cause performance loss due to plugging or fouling. Current research efforts are devoted toward the preparation of cost-effective nickel based catalysts with suppressed carbon formation activity.

Acknowledgements

The authors acknowledge the financial support of SenterNovem and the Dutch Ministry of Economic Affairs (EZ) (EOSLT03015, EOS LT05010 projects). G.D. Elzinga and Ö. Pirgon-Galin are acknowledged for their contribution in the catalyst testing and D. Meyer, M. Sarić and R. Sumbharaju for their contribution in the membrane reformer tests.

References

[1] N.W. Ockwig, T.M. Nenoff, Chem. Rev. 107 (2007) 4078.
[2] G. Manzolini, J.W. Dijkstra, E. Macchi, D. Jansen, Proceedings of the ASME 2006 GT2006, Barcelona, Spain, May, 2006, ASME paper GT2006-90353.
[3] Y.C. van Delft, L.A. Correia, J.P. Overbeek, B. Bongers, P.P.A.C. Pex, Proceedings of the 9th International Conference on Inorganic Membranes-ICIM-9, Lillehammer, Norway, June, 2006.
[4] J.R. Rostrup-Nielsen, in: J.R. Anderson, M. Boudart (Eds.), Catalysis, Science and Technology, vol. 5, Springer-Verlag, Berlin, 1983 (chapter 1).
[5] C.H. Bartholemow, Catal. Rev. Sci. Eng. 24 (1982) 67.
[6] S.N. Paglieri, K.Y. Foo, J.D. Way, J.P. Collins, D.L. Harper-Nixon, Ind. Eng. Chem. Res. 38 (1999) 1925.
[7] K.S. Rothenberger, A.V. Cugini, B.H. Howard, R.P. Killmeyer, M.V. Ciocco, B.D. Morreale, R.M. Enick, F. Bustamante, I.P. Mardilovich, Y.H. Ma, J. Membr. Sci. 244 (2004) 55.
[8] T.A. Peters, M. Stange, H. Klette, R. Bredesen, J. Membr. Sci. 316 (2008) 119.
[9] A. Roine, HSC Chemistry, Outokumpu Research Oy, Pori, Finland, Anon, 2002.
[10] T. Numaguchi, K. Kikuchi, Chem. Eng. Sci. 43 (1988) 2295.
[11] J. Xu, G.F. Froment, AIChE J. 35 (1989) 88.
[12] K. Hou, R. Hughes, Chem. Eng. J. 82 (2001) 311.
[13] J. Wei, E. Iglesia, J. Catal. 225 (2004) 116.
[14] W. Noriaki, S. Kaguei, Heat and Mass Transfer in Packed Beds, Gordon and Breach, New York, 1982.
[15] K.R. Westerterp, W.P.M. Van Swaaij, A.A.C.M. Beenackers, Chemical Reactor Design and Operation, Wiley, Chichester, 1987.
[16] G.S. Madia, G. Barbieri, E. Drioli, Can. J. Chem. Eng. 77 (1999) 698.
[17] J.W. Geus, A.J. Van Dillen, Catalyst Preparation, Deposition–Precipitation Synthesis of Supported Metal Catalysts, 2007, p. 319.
[18] B.C. Bonekamp, A. van Horssen, L.A. Correia, J.F. Vente, W.G. Haije, J. Membr. Sci. 278 (2006) 349.
[19] Y.C. van Delft, L.A. Correia, J.P. Overbeek, D.F. Meyer, A. de Groot, J.W. Dijkstra, D. Jansen, Proceedings of the 8th International Conference Catalysis in Membrane Reactors, Kolkata, India, December, 2007, http://www.ecn.nl/publicaties/default.aspx?nr=ECN-M–08-028.
[20] F.T. Rusting, G.D. Jong, P.P.A.C. Pex, J.A.J. Peters Sealing socket and method for arranging a sealing socket to a tube, International Patent WO 01/63162A1 (2001).
[21] A. Kleinert, G. Grubert, X. Pan, C. Hamel, A. Seidel-Morgenstern, J. Caro, Catal. Today 104 (2005) 267.
[22] G. Chen, L. Hanyi, J. Mater. Sci. Technol. 16 (2000) 88.
[23] K. Hou, R. Hughes, J. Membr. Sci. 206 (2002) 119.
[24] H. Li, A. Goldbach, W. Li, H. Xu, J. Membr. Sci. 299 (2007) 130.
[25] F.C. Gielens, R.J.J. Knibbeler, P.F.J. Duysinx, H.D. Tong, M.A.G. Vorstman, J.T.F. Keurentjes, J. Membr. Sci. 279 (2006) 176.
[26] J.G. McCarty, P.Y. Hou, D. Sheridan, H. Wise, Surface Carbon on Nickel Catalysts, Temperature-Programmed Surface Reaction with Hydrogen and Water, in: ACS Symposium Series, Anon, American Chemical Society, 1982 (chapter 13).